NeuroImage 95 (2014) 176–184

Contents lists available at ScienceDirect

NeuroImage

journal homepage: www.elsevier.com/locate/ynimg

Functional ultrasound imaging reveals different odor-evoked patterns of vascular activity in the main olfactory bulb and the anterior piriform cortex

B.F. Osmanski [a], C. Martin [b], G. Montaldo [a], P. Lanièce [b], F. Pain [b], M. Tanter [a,1], H. Gurden [b,*,1]

[a] Institut Langevin, ESPCI ParisTech, CNRS UMR7587, Inserm U979, Université Paris Diderot 7, 1 rue Jussieu, 75005 Paris, France
[b] Laboratoire d'Imagerie et Modélisation en Neurobiologie et Cancérologie, CNRS UMR8165, Université Paris Diderot 7 et Université Paris Sud, 91405 Orsay France

ARTICLE INFO

Article history:
Accepted 11 March 2014
Available online 24 March 2014

Keywords:
Piriform cortex
Functional ultrasound imaging
Blood volume
Odor activation

ABSTRACT

Topographic representation of the outside world is a key feature of sensory systems, but so far it has been difficult to define how the activity pattern of the olfactory information is distributed at successive stages in the olfactory system. We studied odor-evoked activation patterns in the main olfactory bulb and the anterior piriform cortex of rats using functional ultrasound (fUS) imaging. fUS imaging is based on the use of ultrafast ultrasound scanners and detects variations in the local blood volume during brain activation. It makes deep brain imaging of ventral structures, such as the piriform cortex, possible. Stimulation with two different odors (hexanal and pentylacetate) induced the activation of odor-specific zones that were spatially segregated in the main olfactory bulb. Interestingly, the same odorants triggered the activation of the entire anterior piriform cortex, in all layers, with no distinguishable odor-specific areas detected in the power Doppler images. These fUS imaging results confirm the spatial distribution of odor-evoked activity in the main olfactory bulb, and furthermore, they reveal the absence of such a distribution in the anterior piriform cortex at the macroscopic scale in vivo.

Introduction

Processing of olfactory information is vital for the majority of vertebrates. The olfactory system is built in the same scheme across species, with only two synaptic relays to reach the olfactory cortex from the outside world (Bekkers and Suzuki, 2013). The wiring diagram of the olfactory circuits starts with the olfactory receptor neurons (ORNs), located in the main olfactory epithelium. In the rodent, each ORN, expressing one particular olfactory receptor out of ~1000 (Firestein, 2001; Mombaerts, 2004; Mori and Sakano, 2011), projects out to four glomeruli in the main olfactory bulb (MOB), the first central relay that codes the olfactory information (Shepherd and Greer, 1998). In turn, the MOB transmits the information to the anterior piriform cortex (aPC), the main output structure of the MOB among the primary olfactory cortices. The aPC receives direct and dense sensory input from the mitral/tufted cells (M/TCs) in the MOB from multiple glomerular sources through the lateral olfactory tract (LOT) projection (Apicella et al., 2010; Miyamichi et al., 2011). In addition, different tracing techniques have been used to show that M/TC axons from individual glomeruli were diffusely projecting throughout the aPC (Ghosh et al., 2011; Miyamichi et al., 2011; Sosulski et al., 2011).

Odor-induced spatial maps of the MOB have been characterized extensively (Mori et al., 2006; Murthy, 2011), in particular by in vivo optical imaging (Uchida et al., 2000) and magnetic resonance imaging (MRI) (Xu et al., 2000). A given odorant molecule can activate various subsets of ORNs, which results in a spatially invariant pattern of glomerular activity in the MOB (Belluscio and Katz, 2001; Soucy et al., 2009). Physiological studies have examined the transmission of odor-evoked activities from the MOB to the aPC (Litaudon and Cattarelli, 1996; Poo and Isaacson, 2009; Rennaker et al., 2007; Stettler and Axel, 2009; Suzuki and Bekkers, 2012). These studies have shown that odorants activate sparse groups of neurons that are largely disturbed in all layers of the aPC, without any apparent spatial preference. However, it is not known how odor-evoked activation of different odors is organized in the aPC at the macroscopic scale.

In this study, we used functional ultrasound (fUS) imaging (Macé et al., 2011), a new functional neuroimaging technique based on the use of ultrafast ultrasound scanners, to map odor-evoked activity in the aPC on a large scale. Ultrafast ultrasound scanners have already offered new insights in diagnostic imaging (Tanter et al., 2008) and blood flow imaging under the terminology of "Ultrafast Doppler Imaging" (Bercoff et al., 2011; Osmanski et al., 2012; Udesen et al., 2008). This concept relies on compounded plane wave transmission

Abbreviations: ORNs, olfactory receptor neurons; fUS, functional ultrasound; MOB, main olfactory bulb; aPC, anterior piriform cortex.

* Corresponding author at: Laboratoire IMNC, CNRS UMR8165, Université Paris Diderot et Paris Sud. Bâtiment 440, Université Paris Sud, 91405 Orsay, France. Tel.: +33 169154509.

E-mail address: gurden@imnc.in2p3.fr (H. Gurden).

[1] M.T. and H.G. are co-last authors.

http://dx.doi.org/10.1016/j.neuroimage.2014.03.054
1053-8119/

(Montaldo et al., 2009), which can capture more than 10,000 frames per second compared to the usual 50 frames per second in conventional ultrasound scanners. Thus, Ultrafast Doppler has increased the sensitivity of blood flow measurements by 30-fold (Macé et al., 2013), making the detection of subtle hemodynamic changes in smaller vessels possible compared to conventional Doppler Ultrasound. Similar to other magnetic and optical functional neuroimaging techniques that depend on vascular oxygenation and dynamics (Pain et al., 2011), fUS relies on activity-dependent blood volume changes in small blood vessels to detect active neuronal assemblies in vivo (Macé et al., 2013; Rubin et al., 1995, 1997; Shung et al., 1976). Importantly, fUS was shown to reach an excellent spatiotemporal resolution (below 100 μm and 1 s for a single trial acquisition) in the field of deep brain imaging (Macé et al., 2011).

Using the technical advantages of fUS, we determined how distinct odorants were mapped in two interconnected stations along the olfactory pathway, the MOB and the aPC, on a macroscopic scale. We confirmed the existence of the well-described spatial maps evoked by odor stimulation in the MOB, and we further showed that the aPC is activated as a whole, across all layers, in response to different odorants.

Materials and methods

Animals, surgical procedures and odor delivery

Thirteen adult male Long–Evans rats (Janvier Labs; France) weighing 250–350 g were included in this study. They were housed in collective cages with free access to food and water and maintained under standard conditions (12/12 h light–darkness cycle, 22 °C). All experiments were conducted in accordance with the European Community Council Directive (86/609/EEC). The experimental protocol was controlled and approved by the University Paris-Sud Ethics Committee and the Direction of Veterinary Service (authorization #B91471101).

All rats were anesthetized by an intraperitoneal (i.p.) injection of a mixture of ketamine (60 mg/kg, Imalgene 500®, Merial; France) and medetomidine (0.4 mg/kg, Domitor®, Pfizer Santé Animale; France). Anesthesia was maintained by a periodic i.p. dosage using 1/3 of the initial dose. Body temperature was monitored and maintained at 37 °C using a heating blanket throughout the experiment. Animals were placed in a stereotaxic apparatus for imaging. After an incision in the cranial skin, the bone above the MOB or the aPC was thinned by a dental drill and carefully removed. All image recordings were conducted on freely breathing rats (constant breathing at 1–2 Hz in all rats).

A custom-modified version of a multivial perfusion system (ValveBank 8 II, AutoMate Scientific; USA) attached to an air compressor was used as an olfactometer. A precise volume of the diluted odor (50 μL) was loaded onto a filter paper and placed in a syringe reservoir. Pressure controlled air was delivered through the perfusion system, ensuring a constant rate of odorized air to the animal's nose during valve opening. A mask was placed in front of the rat's nostrils to deliver the odors.

A single activation trial lasted for 48 s. After 6 s of baseline recording under a constant deodorized airflow, one of the two odorants, hexanal 1% or pentylacetate 1% (Sigma-Aldrich; USA), was delivered for 15 s. Another 27 s of air delivery was allowed to recover the baseline value of the metabolic signal. Because the olfactory system is very sensitive to desensitization habituation in the case of repetitive odor stimulations, we allowed at least 3 min of inter-trial interval (ITI). Blank trials, with only air delivered throughout the 48 s, were performed between the odor trials. Four trials per odor were averaged together to obtain functional images of the MOB and the aPC.

To build a recording chamber for each structure, craniotomies were performed according to the MOB and aPC stereotaxic coordinates (Paxinos and Watson, 2007). In a group of five rats, a 5 mm window from 6.5 to 9.5 mm anterior to the bregma was made to give access to the entire MOB. In another group of 8 rats, a 10 mm window was made from 3 to 5 mm anterior to the bregma to give access to the aPC. A silicone gel was applied to the surface of the dura. The gel allows perfect coupling between the ultrasonic probe and the imaged brain region and makes the propagation of ultrasound wave fronts possible. Anteroposterior scans were performed, placing the ultrasound probe on top of these two regions (Fig. 1A). The choice of the ultrasonic image slice with the maximal signal to noise for the power Doppler signal was made taking the shape of the vasculature as a reference (see Fig. 2).

In vivo fUS: images and statistical analysis

fUS was performed using a linear ultrasound probe (192 elements, 20 MHz, 80 μm pitch, and 8 mm elevation focus, Vermon; France) driven by an ultrafast ultrasound scanner (Aixplorer, Supersonic Imagine; France). The biophysics and the technical procedure for fUS were fully explained in our previous reports (Macé et al., 2011, 2013). Briefly, to obtain an ultrasound image of the brain tissue, we used the following ultrafast imaging fUS sequence: i) insonify the brain tissue with a plane wave, ii) record the backscattered echoes coming from a wide-field view on the transducer array, and iii) beamform the raw data to produce an image. In order to ensure a high-quality ultrasound image while preserving an ultrafast frame rate (several 100 s of frames per second), we added several plane wave images coherently (with amplitude and phase) from successive transmissions of tilted plane waves (Montaldo et al., 2009). In this study, the plane wave compounding consisted of coherently adding the images of the brain tissue from 15 different tilted plane waves, with angles varying from −7° to 7° and a 1° step, to compute one high-quality ultrasound image (Fig. 1B). To sample blood flow changes, we repeated this sequence 200 times with a 500 Hz frame rate (corresponding to a 400 ms acquisition time) (Fig. 1C). Because blood moves faster than the tissue, its signal is higher in frequency and can be extracted by time filtering the data with a high-pass filter (4th order Butterworth with a 75 Hz cutoff). One image of power Doppler intensity (which is proportional to the cerebral blood volume, CBV) is obtained by the incoherent temporal mean of the blood signal. Because of the technological computing limitations of our fUS platform (6 CPU core unit, 24 GB RAM), a dead time of 1.1 s is needed to process the power Doppler signal (beamforming and high-pass filtering), resulting in a final temporal sampling rate of 1.5 s per image (Fig. 1D). At the end of this signal processing, we reliably recorded CBV variation in the imaging plane.

Maps of activated pixels were built showing the normalized correlation coefficient r between the local power Doppler signal obtained from fUS and the temporal binary pattern of the odor stimulus. Activation was considered significant for a correlation $r > 2\sigma$, where σ is the spatial standard deviation of the correlation map linked to the noise of the fUS technique. As the volume imaged by fUS covers more than just the brain tissue, σ was computed using at least 100 pixels of the correlation map located outside of the brain. Therefore, this thresholding method can be considered independent of brain activity. The time course for a given region was calculated by averaging the power Doppler signal over time for all pixels in the activated region ($r > 2\sigma$). The intensity of the power Doppler was represented as the percentage of change relative to the baseline in the activated region ± standard deviation (STD). Finally, raw (i.e., not thresholded) hexanal and pentylacetate activation maps in the aPC were compared using the Pearson correlation coefficient.

Results

fUS imaging in the olfactory system

In this study, we investigated the odor-evoked activation of the MOB and the aPC using the fUS technique. We achieved a spatial resolution of 100 μm × 100 μm in the imaging plane, with a slice thickness of 300 μm and a penetration depth (>2 cm) sufficient to image deep brain

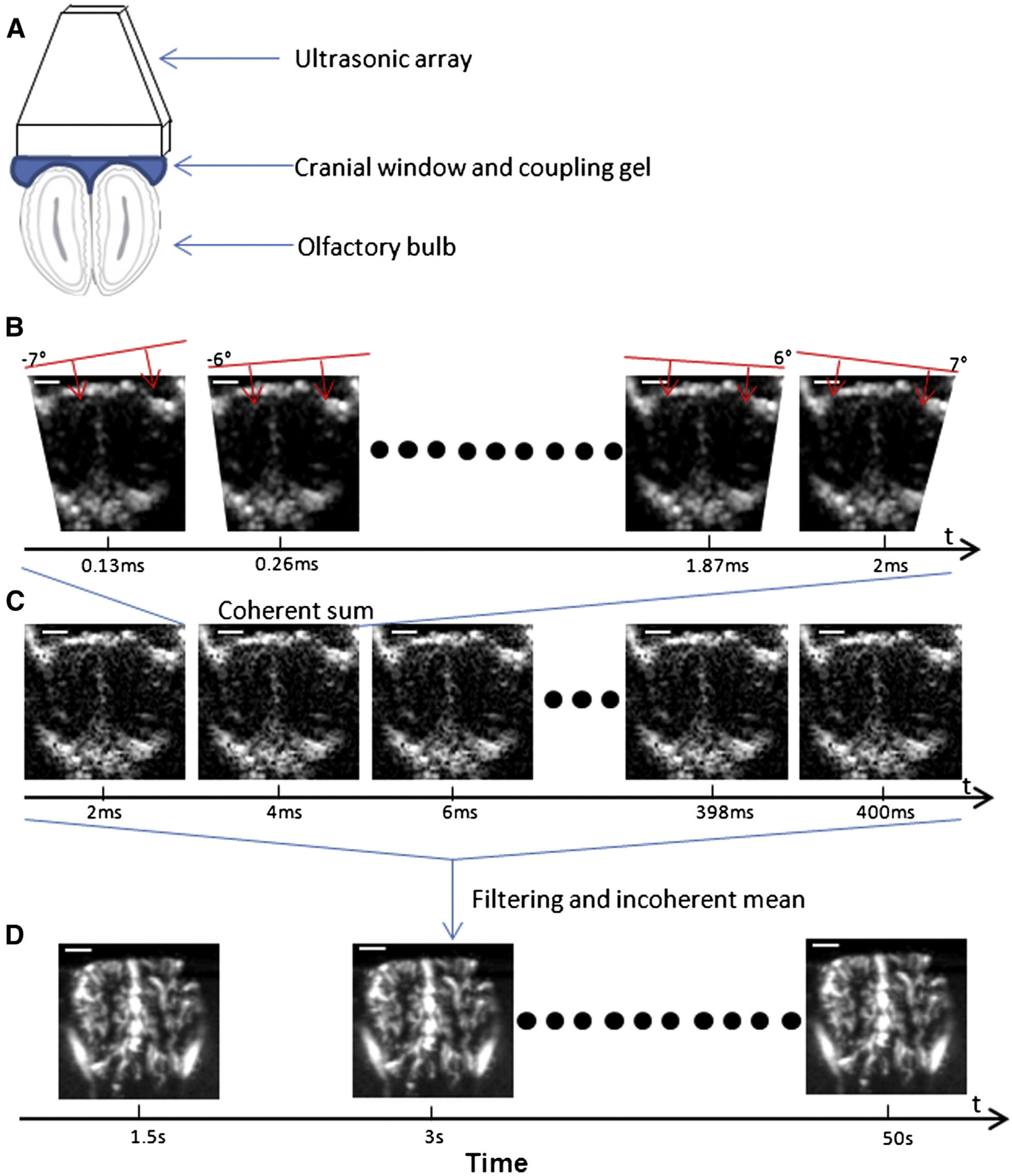

Fig. 1. Protocol for fUS imaging. (A) Experimental setup. The ultrasound probe is placed on top of the MOB after removal of the skull bone. The gel allows for perfect coupling between the ultrasonic probe and the tissue. (B) Plane wave insonification of the brain tissue, with angles varying from −7° to 7° and a 1° step, is performed to record 15 low quality images. After the coherent sum of these 15 images, one quality image of the brain tissue is produced. (C) Repetition of the compounded sequence 200 times with a 500 Hz frame rate results in one Doppler image. (D) One power Doppler intensity image is obtained every 1.5 s during 48 s to measure the spatiotemporal variations of the CBV. For further details see the Materials and methods section.

structures. Doppler scans were performed in the full anteroposterior extent of each structure to observe the overall vascular network (Figs. 1 and 2). Using these images as an anatomical reference, we determined the stereotaxic coordinates to record the fUS for both the MOB and the aPC in a series of preliminary experiments (images not shown). When we performed the actual fUS recording included in our study, we refined the anteroposterior location of the probe to maximize the power Doppler signal. We then probed the odor-evoked vascular activity in a single slice from each structure. To the best of our knowledge, we have produced the first fUS images of the MOB and aPC using in vivo imaging of CBV changes, which permitted us to assess the spatial distribution of the odorant-activated areas in the MOB and the aPC in anesthetized rats.

Odor-evoked activation of the MOB

First, we visualized the vasculature in the MOB, where dense vascular inputs can be observed at the glomerular level (Fig. 2A). Blank trials where only air was delivered to the animal showed no specific activity in the MOB (Fig. 3A). We next mapped specific odor-activated zones

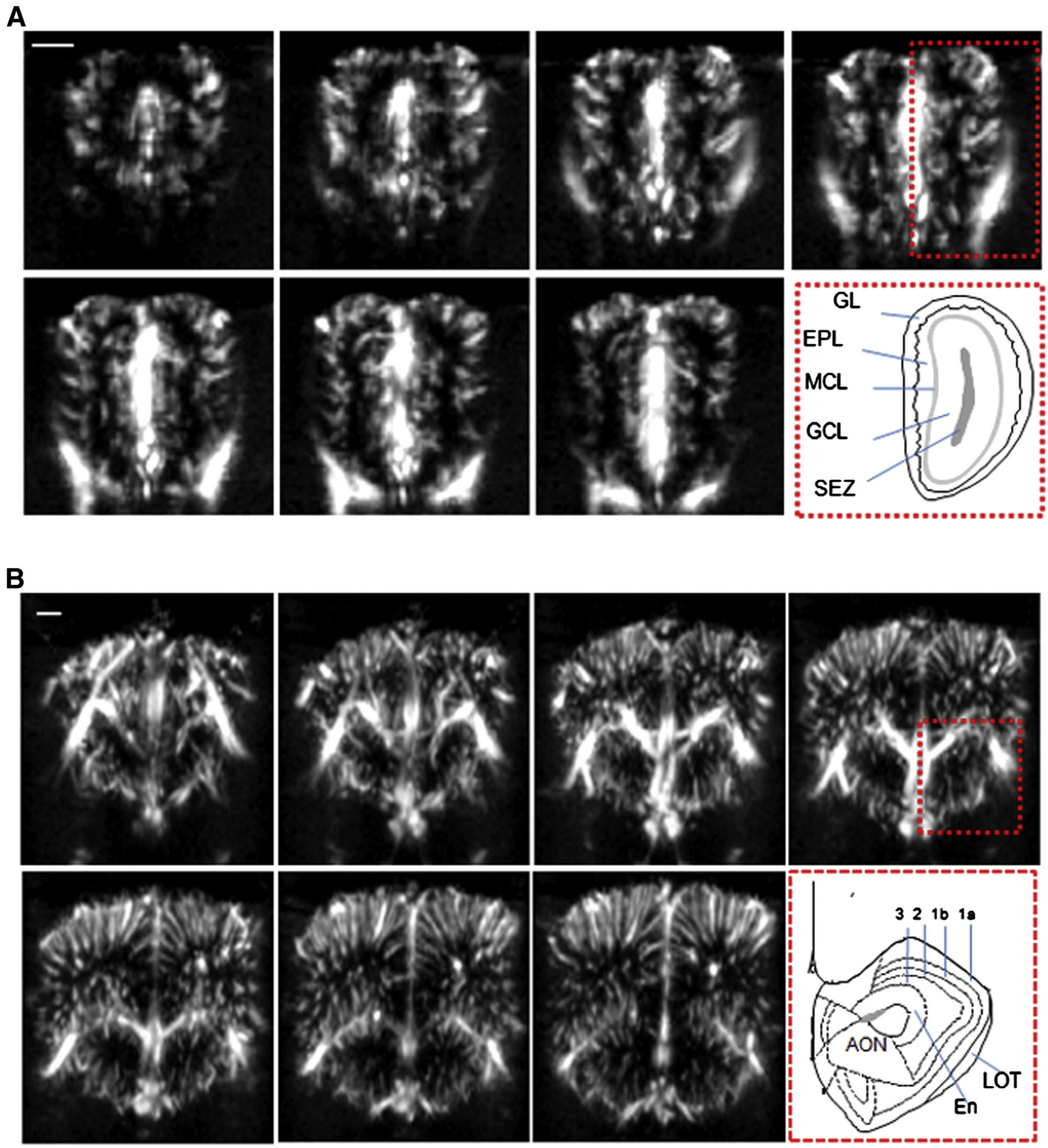

Fig. 2. MOB and aPC vasculature visualized by fUS on 0.3 mm thick coronal slices acquired in the antero-posterior axis (from left to right) in one rat. (A) A dense vascular input is observed in superficial layers of the MOB and decreases in the inner zones. Each image is made with one power Doppler intensity acquisition. The horizontal white bar represents 1 mm. EPL: external plexiform layer. GL: glomerular layer; GCL: granule cell layer; MCL: mitral cell layer; SEZ: subependymal zone. (B) A dense vascular input is observed in all three layers of aPC. The horizontal white bar represents 1 mm. AON: anterior olfactory nucleus. 3, 2, 1b, 1a: layers of aPC. En: endopiriform nucleus. LOT: lateral olfactory tract. Anatomical schemes in (A) and (B) modified from Paxinos and Watson (2007).

(Figs. 3B–D). Artifacts due to respiratory or cardiac movements in the preparation or to spontaneous variation in the vascular activity occasionally occurred during the recordings, but they were efficiently removed from the fUS image using the average of four trials as they happen asynchronously with respect to the stimulus. Interestingly, even one trial was able to produce significant changes enough to allow observation of the power Doppler signal over the background noise in the MOB, as well as record the spatial distribution of activation (Figs. 3B–C). We averaged four trials to obtain an activation map, in an effort to normalize the variability in the reactive areas to odorants that may change from trial to trial (see for example the ventral part of the MOB in response to hexanal in Fig. 3B). We found that both odorants induced specific and symmetrical maps in the MOB (Figs. 3B–C). Hexanal induced further dorsal MOB activity over pentylacetate, which recruited lateral and ventral areas of the MOB when visualized in the same rat (Fig. 3D). Each of the images acquired in Figs. 3B–D is from an independent, representative rat. The odor-evoked power Doppler onset was locked to odor delivery and occurred within 3.00 ± 0.75 s ($n = 5$) after the stimulus onset for both odorants (Fig. 3E). The power Doppler time course was monophasic, meaning that it reached a single peak at 4.50 ± 0.75 s after the odor onset and then returned to baseline. The amplitude of the power Doppler peak relative to the baseline was $12 \pm$

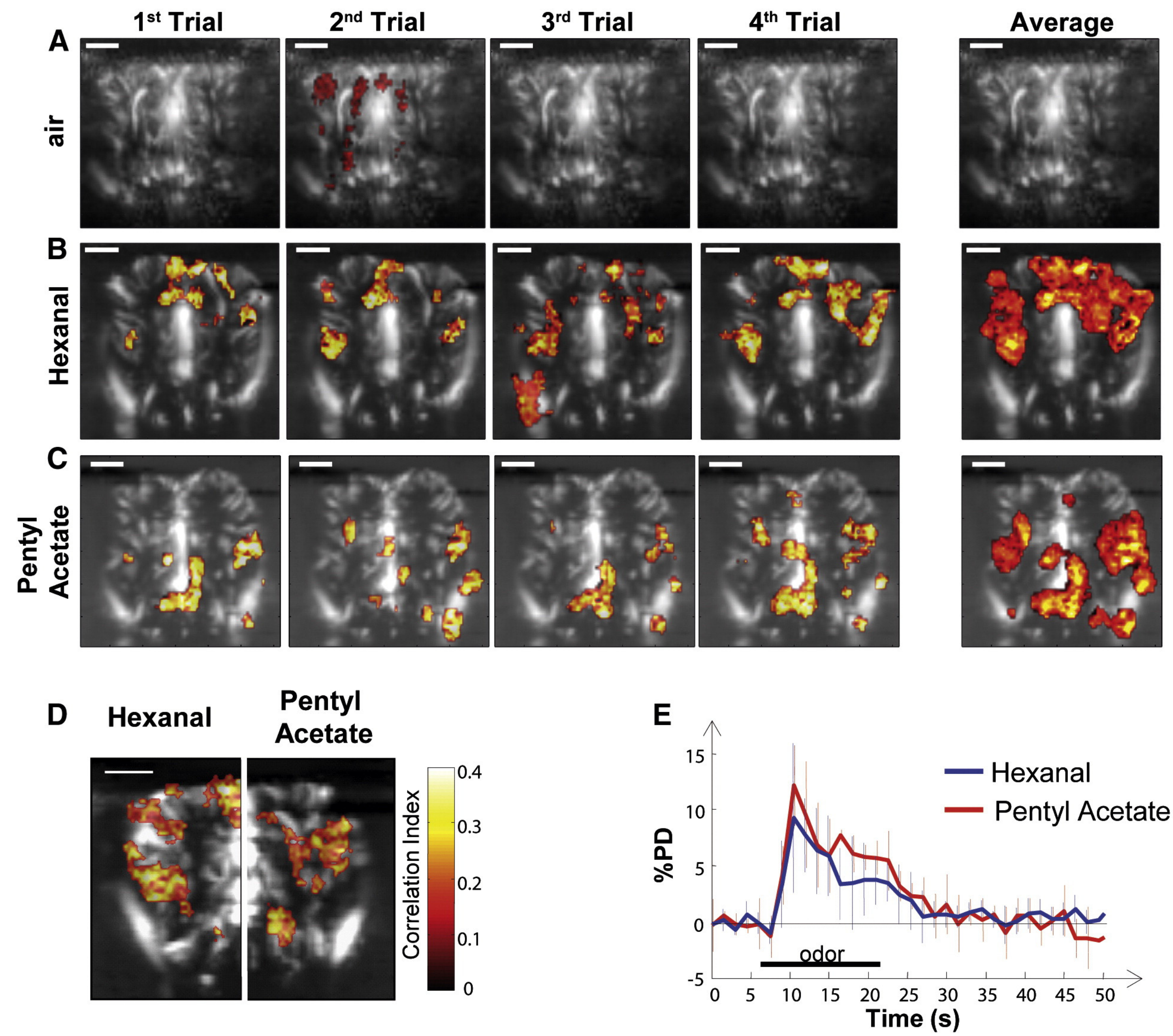

Fig. 3. fUS imaging of odor-evoked activity in the MOB for two different odors. (A) Blank trials in a representative rat. Air stimulation was delivered during the 48 s trial. Four independent trials and the average of these trials are represented. Note that occasionally vascular artifacts occur. The computing of the final correlation map of these four blank trials efficiently excludes these artifacts. (B) Spatial distribution of activity elicited by odor presentation in the MOB for hexanal 1% in a representative rat. The olfactory map is characterized by a precise spatial location and a symmetrical distribution in this coronal view. The horizontal white bar represents 1 mm. (C) Spatial distribution of activity elicited by odor presentation in the MOB for pentyl acetate 1% in one rat that was different from the hexanal trials. B–C, same representation as (A). The horizontal white bar represents 1 mm. (D) Comparison of olfactory maps triggered by the two odorants in the same representative rat. Note that hexanal-induced signals are more dorsal than the pentylacetate-induced ones. Each image is the average of four odor trials acquired in the same rat (different from the rats shown in B and C). The horizontal white bar represents 1 mm. (E) Time course of sensory-evoked activity in the MOB. Both odors induce the same power Doppler dynamics in terms of time course and amplitude. Each curve is the average of four odor trials (n = 5 rats).

3% and 10 ± 6% for pentylacetate (n = 5) and hexanal (n = 5, same animal as with the pentylacetate), respectively (Fig. 3E).

Odor-evoked activation of the aPC

Our modified fUS technique also made it possible to record aPC activation. Dense vascular inputs can be visualized in the three layers of the aPC (Fig. 2B). Functional images are represented in Fig. 4, which has the same format as Fig. 3. aPC did not present a patchy pattern of activation in response to the different odorants. On the contrary, we always observed a global, widespread odor activation that covered all of the layers (Figs. 4B–E). Each of the images acquired in Figs. 4B–D is from an independent, representative rat. In the aPC, the hexanal and pentylacetate maps were highly correlated (Pearson correlation coefficient = 0.53 ± 0.08, $p < 0.001$, n = 8), meaning that the aPC maps for these odorants highly overlapped. The odor-evoked Doppler onset in the aPC was locked to odor delivery and occurred within 3.00 ± 0.75 s (n = 8) after the stimulus onset for both odorants (Fig. 4E). The power Doppler time course recorded in the aPC presented multiple peaks of activity. The first peak occurred within 4.5 ± 0.75 s after the odor onset for both stimuli (n = 8, same rats used for both hexanal and pentylacetate, Fig. 4E). It reached a normalized amplitude of 5 ± 2% and 7 ± 3% for pentylacetate (n = 8) and hexanal (n = 8), respectively. The second peak occurred at 18 ± 0.75 s for pentylacetate (n = 8) and 19.5 ± 0.75 s for hexanal (n = 8 same rats used in both experiments) after odor onset (Fig. 4E), with a normalized amplitude of 6 ± 3% for pentylacetate (n = 8) and 7 ± 2% for hexanal (n = 8) (Fig. 4E).

Discussion

Understanding how the functional connectivity to higher order sensory processing regions is distributed has profound implications for the way that odors are perceived. Recent work has revealed that odors are

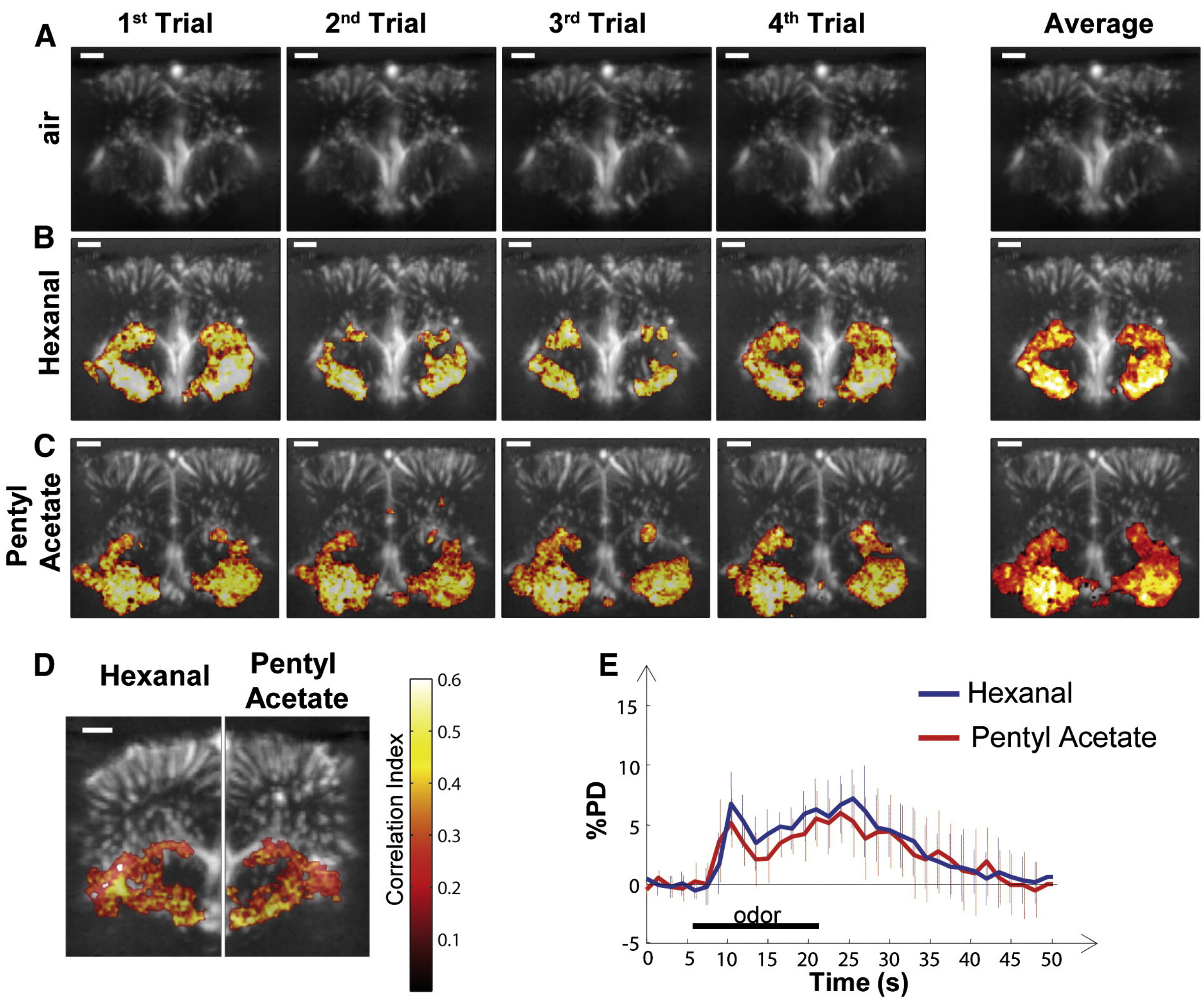

Fig. 4. fUS imaging of odor-evoked activity in the aPC for two different odors. (A) Blank trial in a representative rat. Same representation as in Fig. 3A. (B) Spatial distribution of activity elicited by odor presentation in the aPC for hexanal 1% in a representative rat. Note the absence of any specific zone of activity compared to MOB mapping in Fig. 3B. (C) Spatial distribution of activity elicited by odor presentation in the aPC for pentylacetate 1% in one rat (different rat from the hexanal trials). Note that the distribution of activity highly overlaps between the hexanal and pentylacetate treatments. The horizontal white bar represents 1 mm. (D) Spatial distribution of activity elicited by odor presentation in the aPC for hexanal 1% and pentylacetate 1% in one representative rat. All layers of the aPC are diffusely activated by the two odorants. Each image is the average of four odor trials in the same rat (different from the rats shown in B and C). The horizontal white bar represents 1 mm. (E) Both odors induce the same power Doppler dynamics in the aPC. In contrast to MOB activation, the aPC time course is characterized by multiple peaks of activity. Each curve is the average of four odor trials (n = 8 rats).

sparsely represented in the aPC, at the level of a single neuron (Poo and Isaacson, 2009; Stettler and Axel, 2009). Using fUS to probe activation at the macroscopic level, we demonstrated that the spatial organization in the MOB is not conserved in the aPC; activation in the aPC is widespread in response to an odor and not distinguishable between different odors.

fUS imaging technique: a new tool to sample activity-dependent vascular changes in the brain

fUS is a new technique that was used to visualize the activation of the somatosensory cortex in response to paw stimulation (Macé et al., 2011). An exhaustive review on the advantages and limitations of fUS imaging has recently been published (Macé et al., 2013). The following are the main points to consider with this technique, in the context of olfactory imaging.

The spatial resolution of the fUS technique is the actual resolution of the ultrafast plane wave imaging. In ultrasound imaging, the lateral and the depth resolution correspond to the wavelength used for imaging. In our case, since the frequency was 15 MHz and the speed of sound was 1540 m/s, the wavelength was 100 μm. Thus, the resolution in depth and in the lateral direction was 100 μm. The resolution in the ultrasound plane of ultrafast imaging (both lateral resolution and axial resolution) does not vary with depth (Denarie et al., 2013; Montaldo et al., 2009). The resolution in the elevation plane is set by a geometrical focal acoustic lens and by the shape of the ultrasound wave field and could vary with depth. This resolution was measured and ranges between 300 μm at the focal distance of the geometrical focal lens (8 mm from the probe) and 400 μm on the upper and lower edges of the imaging field. In order to optimize the slice thickness, the geometrical focus was placed in the middle of the MOB or the aPC.

For MOB imaging, the fUS spatial resolution (in-plane resolution 100 $*$ 100 μm with a slice thickness of 300 μm) is comparable to Blood Oxygen Level Dependent (BOLD)-fMRI (200 $*$ 200 μm with a slice thickness of 250 μm in Xu et al., 2000). However, compared to BOLD-fMRI, fUS provides easier access to a functional neuroimaging system, in terms of financial cost, portability (the fUS machine is transportable and installed on wheels), and technical combination (easier multimodality with electrophysiology, Macé et al., 2011). Owing to its penetration depth (>2 cm), fUS can record vascular signals from ventral cortices in the rodent brain, such as the aPC.

fUS does suffer from some limitations that can be overcome in the future. Similar to optical and MR imaging techniques using vascular signals, a central question is the compartmental origin of the power Doppler signal. The fUS signal is proportional to the number of moving red blood cells (RBCs) in the recorded voxel (Shung et al., 1976). The proportionality of the power Doppler signal to the blood volume (Rubin et al., 1995, 1997) is valid if the hematocrit is considered constant and if we disregard the possible variations in RBC backscattering properties. In theory, fUS could be sensitive to any moving objects that scatter from the brain tissue signal and/or from the blood. To specifically access hemodynamics, the signal coming from the brain tissue has to be subtracted with a high-pass filter (called clutter filtering in the ultrasound field). However, clutter filtering limits the signal from slow blood flow (RBCs with an axial velocity less than 4 mm/s are not recorded). Because two-photon fluorescence light microscopy imaging showed a velocity of 0.8 mm/s in the MOB (Chaigneau et al., 2003), which corresponds to the average capillary velocity (Kleinfeld et al., 1998), fUS cannot detect variations in blood vessels with slow dynamics, such as the capillary bed. Arterioles present a blood flow ten times superior to capillaries (Dirnagl et al., 1992; Petzold et al., 2008; Shih et al., 2009). Thus, fUS is particularly sensitive to hemodynamics in arterioles participating in functional hyperemia, defined as the matched increase in neuronal activity and local hemodynamics (Petzold and Murthy, 2011). For the time being, arterioles are the prime source for the power Doppler signal. As in other techniques dependent on blood dynamics, such as optical imaging and BOLD-fMRI (Kim and Ogawa, 2012), the cellular triggers and vascular origins of power Doppler signals must be further explored (Macé et al., 2013). In this context, the relationship between hematocrit and changes in CBV and CBF during sensory activation must also be explored.

Another issue with fUS, as in other imaging techniques, is signal processing. In this study, we efficiently proceeded with a thresholding technique that used a correlation method with a standard square-wave model based on the shape of the stimulus. With this type of processing, we obtained reproducible activation maps. Because the odor-evoked vascular response in the aPC has a complex shape (characterized by several peaks) and no model for aPC hemodynamics is available in the literature, we decided against using a more sophisticated thresholding method. In the close future, improvements in the signal processing of power Doppler signals are expected, with a better knowledge of hemodynamics in response to odors in the aPC. In particular, to suppress the 1.1 s dead time currently necessary for signal processing and to increase the temporal resolution in power Doppler signal acquisition, the new generation of high-end graphics processing unit boards will be incorporated into the future version of the fUS imaging set-up. This technical improvement will make the real-time processing of power Doppler signals and high temporal resolution for the follow-up of hemodynamics possible.

Presently, fUS requires anesthesia and a craniotomy. A craniotomy induces changes in the intracranial pressure that could impact the local vasculature. However, the intracranial pressure changes induced by local skull removal are not likely to significantly influence the sensory-evoked vascular signals since the olfactory maps recorded using IOS with a thinned bone overlying the MOB or without bone and dura have resulted in the same maps (Wachowiak and Cohen, 2003). In addition, in our experiments the dura was kept intact during fUS in the MOB and the aPC, and we could reliably record power Doppler signals in the dorsal MOB close to the site of the craniotomy (see Fig. 2B). Anesthesia partially inhibits vascular reactivity (Desai et al., 2011), as well as cellular mechanisms responsible for functional hyperemia (Thrane et al., 2012). However, neurovascular coupling is still present in acute preparations (Franceschini et al., 2010). Indeed, anesthetics are widely used in the olfactory field for imaging of vascular signals in vivo. Urethane (Lecoq et al., 2009; Petzold et al., 2008; Soucy et al., 2009; Xu et al., 2000), pentobarbital (Vincis et al., 2012; Wachowiak and Cohen, 2003), thiopental (Rubin and Katz, 1999; Uchida et al., 2000), and ketamine (Chery et al., 2011; Lecoq et al., 2009; Soucy et al., 2009; Gurden et al., 2006) were successfully used to image the MOB and detected the same specific activated regions in response to the same odorants. Although we consider a ketamine-anesthetized preparation appropriate for fUS imaging of the olfactory system, running non-invasive fUS imaging in awake, restrained rodents is clearly the next technical step.

Activation of odor-evoked spatial modules in the MOB recorded by fUS

fUS was previously used to image whisker-evoked cortical and thalamic responses in the rat brain (Macé et al., 2011). Here we recorded specific odor-activated zones in the MOB in response to two different odorants, confirming what has been shown by intrinsic optical signal imaging (Pain et al., 2011; Uchida et al., 2000) and fMRI (Xu et al., 2000) in vivo. For example, we observed that contrary to pentylacetate, hexanal activates the dorsal surface of the MOB. This is consistent with results found by other imaging techniques that studied MOB maps triggered by aldehydes such as hexanal (Johnson and Leon, 2000) versus acetates such as pentylacetate (Johnson et al., 1998). Therefore, our MOB images validate fUS for use in olfactory imaging. Furthermore, because (i) there is still much to understand about spatial coding of bulbar input to the aPC at the macroscopic scale and (ii) fUS has the advantage of sampling deep areas in the brain, we applied it to efficiently image aPC activation in response to different odorants in vivo.

Odor-evoked widespread vascular activity in aPC layers recorded by fUS

A topographic organization based on spatial domains is present in all sensory cortices of mammals. Spatial information in the peripheral sense organ is maintained by the cortex and has been demonstrated by several techniques, including optical and MR imaging. For example, whiskers are represented by maps within the barrels of the somatosensory cortex (Petersen, 2007), and there is a retinotopic organization of the visual cortex (Schuett et al., 2002). However, our data indicated a widespread increase in CBV in all aPC layers in response to different odorants. Thus, according to our results which complement previous data (Poo and Isaacson, 2009; Stettler and Axel, 2009), odor-evoked aPC representations differ from those of other neocortical sensory areas such as V1 or the barrel cortex, where cells are tuned for stimulus features and show macroscopic spatial patterning. It remains to be seen what the cellular origins of such a broad odor-evoked activation in the aPC could be.

Recurrent broadly distributed odor-evoked activity in the aPC at the macroscopic scale

The power Doppler signals that we recorded in the aPC presented a reverberating activity, with multiple peaks in all layers. Interestingly, the second peak of activity (~18 s after odor onset) occurred in the aPC long after the first one (~4 s after odor onset), which was concomitant with the single peak characterizing MOB activity. The odor-evoked time course of vascular activity recorded in the aPC could be due to the recurrent excitatory–inhibitory networks that were characterized within this structure (Franks et al., 2011; Poo and Isaacson, 2009). Anatomically, inputs from the MOB arrive through the LOT and make synapses with dendrites of the aPC cells in layer 1a, whereas dense corticocortical association synapses are made in layer 1b (Bekkers and Suzuki, 2013; Haberly, 2001; Isaacson, 2010). Layers 2 and 3 contain the cell bodies of pyramidal cells (Bekkers and Suzuki, 2013; Haberly, 2001; Isaacson, 2010). Interneurons are present in all layers (Bekkers and Suzuki, 2013). Functionally, extracellular spike recordings have found that cells activated by a particular odor are distributed widely in the aPC (Litaudon et al., 2003; Rennaker et al., 2007). More recent studies have shown that a maximum of 15% of the pyramidal PC cells sampled with either patch clamp (Poo and Isaacson, 2009) or optical imaging (Stettler and Axel, 2009) is activated in response to an odorant. In addition, these recent studies revealed long-range excitatory connections to at least 2000 cells per cortical cell within the aPC. Therefore, this extensive recurrent circuitry might be responsible for the global activity of the aPC. Still, global inhibition in the aPC (Franks et al., 2011; Poo and Isaacson, 2011; Suzuki and Bekkers, 2010, 2012; Zhan and Luo, 2010), which is broadly tuned, may also be responsible for the global activity detected in our fUS images: the fast spiking activity of inhibitory interneurons requires strong energetic inputs (Buzsáki et al., 2007) and specific classes of interneurons control local hemodynamics (Cauli et al., 2004). Describing the precise cellular mechanisms underlying fUS signals in the aPC, and particularly the role of inhibitory interneurons (Stokes and Isaacson, 2010; Suzuki and Bekkers, 2007), will be a major challenge for future fUS studies.

Conclusion

Using fUS to follow olfactory activation, we showed that the aPC presents a widespread activation in response to different odors. fUS is a technique well-suited to bring further insights to the understanding of olfactory processing in the aPC. Further experiments are needed to assess whether widespread activation of the aPC occurs for mixtures of odorants (Stettler and Axel, 2009; Yoshida and Mori, 2007) and if this activation may be refined with learning (Choi et al., 2011; Litaudon et al., 2003; Saar and Barkai, 2009).

Conflict of interest statement

The authors have no conflict of interest to declare.

Acknowledgements

This work was partly supported by the Agence Nationale de la Recherche under the program ‘‘Future Investments’’ with the reference ANR-10-EQPX-15. C.M., F.P. and H.G. are part of the "Ecole des Neurosciences Paris Ile de France" network.

References

Apicella, A., Yuan, Q., Scanziani, M., Isaacson, J.S., 2010. Pyramidal cells in piriform cortex receive convergent input from distinct olfactory bulb glomeruli. J. Neurosci. 30, 14255–14260.
Bekkers, J.M., Suzuki, N., 2013. Neurons and circuits for odor processing in the piriform cortex. Trends Neurosci. 26, 429–438.
Belluscio, L., Katz, L.C., 2001. Symmetry, stereotypy, and topography of odorant representations in mouse olfactory bulbs. J. Neurosci. 21, 2113–2122.
Bercoff, J., Montaldo, G., Loupas, T., Savery, D., Mézière, F., Fink, M., Tanter, M., 2011. Ultrafast compound Doppler imaging: providing full blood flow characterization. IEEE Trans. Ultrason. Ferroelectr. Freq. Control 58, 134–147.
Buzsáki, G., Kaila, K., Raichle, M., 2007. Inhibition and brain work. Neuron 56, 771–783.
Cauli, B., Tong, X.K., Rancillac, A., Serluca, N., Lambolez, B., Rossier, J., Hamel, E., 2004. Cortical GABA interneurons in neurovascular coupling: relays for subcortical vasoactive pathways. J. Neurosci. 24, 8940–8949.
Chaigneau, E., Oheim, M., Audinat, E., Charpak, S., 2003. Two-photon imaging of capillary blood flow in olfactory bulb glomeruli. Proc. Natl. Acad. Sci. U. S. A. 100, 13081–13086.
Chery, R., L'Heureux, B., Bendahmane, M., Renaud, R., Martin, C., Pain, F., Gurden, H., 2011. Imaging odor-evoked activities in the mouse olfactory bulb using optical reflectance and autofluorescence signals. J. Vis. Exp. e3336.
Choi, G.B., Stettler, D.D., Kallman, B.R., Bhaskar, S.T., Fleischmann, A., Axel, R., 2011. Driving opposing behaviors with ensembles of piriform neurons. Cell 146, 1004–1015.
Denarie, B., Tangen, T.A., Ekroll, I.K., Rolim, N., Torp, H., Bjåstad, T., Lovstakken, L., 2013. Coherent plane wave compounding for very high frame rate ultrasonography of rapidly moving targets. IEEE Trans. Med. Imaging 32, 1265–1276.
Desai, M., Kahn, I., Knoblich, U., Bernstein, J., Atallah, H., Yang, A., Kopell, N., Buckner, R.L., Graybiel, A.M., Moore, C.I., Boyden, E.S., 2011. Mapping brain networks in awake mice using combined optical neural control and fMRI. J. Neurophysiol. 105, 1393–1405.
Dirnagl, U., Villringer, A., Einhäupl, K.M., 1992. In-vivo confocal scanning laser microscopy of the cerebral microcirculation. J. Microsc. 165, 147–157.
Firestein, S., 2001. How the olfactory system makes sense of scents. Nature 413, 211–218.
Franceschini, M.A., Radhakrishnan, H., Thakur, K., Wu, W., Ruvinskaya, S., Carp, S., Boas, D. A., 2010. The effect of different anesthetics on neurovascular coupling. Neuroimage 51, 1367–1377.
Franks, K.M., Russo, M.J., Sosulski, D.L., Mulligan, A.A., Siegelbaum, S.A., Axel, R., 2011. Recurrent circuitry dynamically shapes the activation of piriform cortex. Neuron 72, 49–56.
Ghosh, S., Larson, S.D., Hefzi, H., Marnoy, Z., Cutforth, T., Dokka, K., Baldwin, K.K., 2011. Sensory maps in the olfactory cortex defined by long-range viral tracing of single neurons. Nature 472, 217–220.
Gurden, H., Uchida, N., Mainen, Z., 2006. Sensory-evoked intrinsic optical signals in the olfactory bulb are coupled to glutamate release and uptake. Neuron 52, 335–345.
Haberly, L.B., 2001. Parallel-distributed processing in olfactory cortex: new insights from morphological and physiological analysis of neuronal circuitry. Chem. Senses 26, 551–576.
Isaacson, J.S., 2010. Odor representations in mammalian cortical circuits. Curr. Opin. Neurobiol. 20, 328–331.
Johnson, B.A., Leon, M., 2000. Modular representations of odorants in the glomerular layer of the rat olfactory bulb and the effects of stimulus concentration. J. Comp. Neurol. 422, 496–509.
Johnson, B.A., Woo, C.C., Leon, M., 1998. Spatial coding of odorant features in the glomerular layer of the rat olfactory bulb. J. Comp. Neurol. 393, 457–471.
Kim, S.G., Ogawa, S., 2012. Biophysical and physiological origins of blood oxygenation level-dependent fMRI signals. J. Cereb. Blood Flow Metab. 32, 1188–1206.
Kleinfeld, D., Mitra, P.P., Helmchen, F., Denk, W., 1998. Fluctuations and stimulus-induced changes in blood flow observed in individual capillaries in layers 2 through 4 of rat neocortex. Proc. Natl. Acad. Sci. U. S. A. 95, 15741–15746.
Lecoq, J., Tiret, P., Najac, M., Shepherd, G.M., Greer, C.A., Charpak, S., 2009. Odor-evoked oxygen consumption by action potential and synaptic transmission in the olfactory bulb. J. Neurosci. 29, 1424–1433.
Litaudon, P., Cattarelli, M., 1996. Olfactory bulb repetitive stimulations reveal non-homogeneous distribution of the inhibitory processes in the rat piriform cortex. Eur. J. Neurosci. 8, 21–29.
Litaudon, P., Amat, C., Bertrand, B., Vigouroux, M., Buonviso, N., 2003. Piriform cortex functional heterogeneity revealed by cellular responses to odours. Eur. J. Neurosci. 17, 2457–2461.
Macé, E., Montaldo, G., Cohen, I., Baulac, M., Fink, M., Tanter, M., 2011. Functional ultrasound imaging of the brain. Nat. Methods 8, 662–664.
Macé, E., Montaldo, G., Osmanski, B.F., Cohen, I., Fink, M., Tanter, M., 2013. Functional ultrasound imaging of the brain: theory and basic principles. IEEE Trans. Ultrason. Ferroelectr. Freq. Control 60, 492–506.
Miyamichi, K., Amat, F., Moussavi, F., Wang, C., Wickersham, I., Wall, N.R., Taniguchi, H., Tasic, B., Huang, Z.J., He, Z., Callaway, E.M., Horowitz, M.A., Luo, L., 2011. Cortical representations of olfactory input by trans-synaptic tracing. Nature 472, 191–196.
Mombaerts, P., 2004. Genes and ligands for odorant, vomeronasal and taste receptors. Nat. Rev. Neurosci. 5, 263–278.
Montaldo, G., Tanter, M., Bercoff, J., Benech, N., Fink, M., 2009. Coherent plane-wave compounding for very high frame rate ultrasonography and transient elastography. IEEE Trans. Ultrason. Ferroelectr. Freq. Control 56, 489–506.
Mori, K., Sakano, H., 2011. How is the olfactory map formed and interpreted in the mammalian brain? Annu. Rev. Neurosci. 34, 467–499.
Mori, K., Takahashi, Y.K., Igarashi, K.M., Yamaguchi, M., 2006. Maps of odorant molecular features in the mammalian olfactory bulb. Physiol. Rev. 86, 409–433.
Murthy, V.N., 2011. Olfactory maps in the brain. Annu. Rev. Neurosci. 34, 233–258.
Osmanski, B.F., Pernot, M., Montaldo, G., Bel, A., Messas, E., Tanter, M., 2012. Ultrafast Doppler imaging of blood flow dynamics in the myocardium. IEEE Trans. Med. Imaging 31, 1661–1668.
Pain, F., L'heureux, B., Gurden, H., 2011. Visualizing odor representation in the brain: a review of imaging techniques for the mapping of sensory activity in the olfactory glomeruli. Cell. Mol. Life Sci. 68, 2689–2709.
Paxinos, G., Watson, C., 2007. The Rat Brain in Stereotaxic Coordinates, 6th ed. Academic Press, Elsevier Inc., San Diego.
Petersen, C.C., 2007. The functional organization of the barrel cortex. Neuron 56, 339–355.
Petzold, G.C., Murthy, V.N., 2011. Role of astrocytes in neurovascular coupling. Neuron 71, 782–797.
Petzold, G., Albeanu, D., Sato, T., Murthy, V., 2008. Coupling of neural activity to blood flow in olfactory glomeruli is mediated by astrocytic pathways. Neuron 58, 897–910.
Poo, C., Isaacson, J.S., 2009. Odor representations in olfactory cortex: "sparse" coding, global inhibition, and oscillations. Neuron 62, 850–861.
Poo, C., Isaacson, J.S., 2011. A major role for intracortical circuits in the strength and tuning of odor-evoked excitation in olfactory cortex. Neuron 72, 41–48.
Rennaker, R.L., Chen, C.F., Ruyle, A.M., Sloan, A.M., Wilson, D.A., 2007. Spatial and temporal distribution of odorant-evoked activity in the piriform cortex. J. Neurosci. 27, 1534–1542.
Rubin, B.D., Katz, L.C., 1999. Optical imaging of odorant representations in the mammalian olfactory bulb. Neuron 23, 499–511.
Rubin, J.M., Adler, R.S., Fowlkes, J.B., Spratt, S., Pallister, J.E., Chen, J.F., Carson, P.L., 1995. Fractional moving blood volume: estimation with power Doppler US. Radiology 197, 183–190.
Rubin, J.M., Bude, R.O., Fowlkes, J.B., Spratt, R.S., Carson, P.L., Adler, R.S., 1997. Normalizing fractional moving blood volume estimates with power Doppler US: defining a stable intravascular point with the cumulative power distribution function. Radiology 205, 757–765.
Saar, D., Barkai, E., 2009. Long-lasting maintenance of learning-induced enhanced neuronal excitability: mechanisms and functional significance. Mol. Neurobiol. 39, 171–177.
Schuett, S., Bonhoeffer, T., Hübener, M., 2002. Mapping retinotopic structure in mouse visual cortex with optical imaging. J. Neurosci. 22, 6549–6559.
Shepherd, G.M., Greer, C.A., 1998. The olfactory bulb. In: Shepherd, G.M. (Ed.), The Synaptic Organization of the Brain. Oxford University Press, New York, pp. 159–203.
Shih, A.Y., Friedman, B., Drew, P.J., Tsai, P.S., Lyden, P.D., Kleinfeld, D., 2009. Active dilation of penetrating arterioles restores red blood cell flux to penumbral neocortex after focal stroke. J. Cereb. Blood Flow Metab. 29, 738–751.
Shung, K.K., Sigelmann, R.A., Reid, J.M., 1976. Scattering of ultrasound by blood. IEEE Trans. Biomed. Eng. 23, 460–467.

Sosulski, D.L., Bloom, M.L., Cutforth, T., Axel, R., Datta, S.R., 2011. Distinct representations of olfactory information in different cortical centres. Nature 472, 213–216.
Soucy, E.R., Albeanu, D.F., Fantana, A.L., Murthy, V.N., Meister, M., 2009. Precision and diversity in an odor map on the olfactory bulb. Nat. Neurosci. 12, 210–220.
Stettler, D.D., Axel, R., 2009. Representations of odor in the piriform cortex. Neuron 63, 854–864.
Stokes, C.C., Isaacson, J.S., 2010. From dendrite to soma: dynamic routing of inhibition by complementary interneuron microcircuits in olfactory cortex. Neuron 67, 452–465.
Suzuki, N., Bekkers, J.M., 2007. Inhibitory interneurons in the piriform cortex. Clin. Exp. Pharmacol. Physiol. 34, 1064–1069.
Suzuki, N., Bekkers, J.M., 2010. Distinctive classes of GABAergic interneurons provide layer-specific phasic inhibition in the anterior piriform cortex. Cereb. Cortex 20, 2971–2984.
Suzuki, N., Bekkers, J.M., 2012. Microcircuits mediating feedforward and feedback synaptic inhibition in the piriform cortex. J. Neurosci. 32, 919–931.
Tanter, M., Bercoff, J., Athanasiou, A., Deffieux, T., Gennisson, J.L., Montaldo, G., Muller, M., Tardivon, A., Fink, M., 2008. Quantitative assessment of breast lesion viscoelasticity: initial clinical results using supersonic shear imaging. Ultrasound Med. Biol. 34, 1373–1386.
Thrane, A.S., Rangroo Thrane, V., Zeppenfeld, D., Lou, N., Xu, Q., Nagelhus, E.A., Nedergaard, M., 2012. General anesthesia selectively disrupts astrocyte calcium signaling in the awake mouse cortex. Proc. Natl. Acad. Sci. U. S. A. 109, 18974–18979.
Uchida, N., Takahashi, Y.K., Tanifuji, M., Mori, K., 2000. Odor maps in the mammalian olfactory bulb: domain organization and odorant structural features. Nat. Neurosci. 3, 1035–1043.
Udesen, J., Gran, F., Hansen, K.L., Jensen, J.A., Thomsen, C., Nielsen, M.B., 2008. High frame-rate blood vector velocity imaging using plane waves: simulations and preliminary experiments. IEEE Trans. Ultrason. Ferroelectr. Freq. Control 55, 1729–1743.
Vincis, R., Gschwend, O., Bhaukaurally, K., Beroud, J., Carleton, A., 2012. Dense representation of natural odorants in the mouse olfactory bulb. Nat. Neurosci. 15, 537–539.
Wachowiak, M., Cohen, L.B., 2003. Correspondence between odorant-evoked patterns of receptor neuron input and intrinsic optical signals in the mouse olfactory bulb. J. Neurophysiol. 89, 1623–1639.
Xu, F., Kida, I., Hyder, F., Shulman, R.G., 2000. Assessment and discrimination of odor stimuli in rat olfactory bulb by dynamic functional MRI. Proc. Natl. Acad. Sci. U. S. A. 97, 10601–10606.
Yoshida, I., Mori, K., 2007. Odorant category profile selectivity of olfactory cortex neurons. J. Neurosci. 27, 9105–9114.
Zhan, C., Luo, M., 2010. Diverse patterns of odor representation by neurons in the anterior piriform cortex of awake mice. J. Neurosci. 30, 16662–16672.